various cellular disorders. Thus, these abnormal aggregates are required for rapid degradation (33, 34). Recruitment of chaperones is an adaptive cellular response to assist in ubiquitin-dependent degradation. Hsp72 is usually expressed at low basal levels and increases in response to cellular stressors, therefore, the up-regulation and recruitment to IBs of Hsp72 indicates that the formation of abnormal structures consisting of massive viral proteins is deleterious for cell survival. Indeed, our data revealed that Hsp72 bound to the P protein through its C-terminal peptide binding domain and promoted the ubiquitin-proteasomal degradation of P protein, and suppressed apoptotic cell death of MuV-infected cells. Because the accumulation of the ubiquitinated P protein had no effect on viral propagation, Hsp72 might contribute to the degradation of excess amounts of P protein. It is unclear why the P protein, but not N protein, is targeted by Hsp72-mediated degradation. However, these data may suggest a specific role for the P protein degradation in cellular stress responses. One possibility is speculated as follows: the specific degradation of MuV P protein may elicit a high-avidity cytotoxic T lymphocyte (CTL) response, since the degraded paramyxoviral P protein but not other viral proteins has been reported to contribute to effective CTL elicitation via MHC class I presentation (35, 36). Although we did not examine the possibility in this study, Hsp72 might play a crucial role in elicitation of high-avidity CTLs by regulating the ubiquitin-proteasomal degradation of MuV P protein.

Hsp70 family chaperone proteins play major roles in protein quality control (PQC) and maintenance of protein homeostasis. They not only support correct folding and re-folding of client proteins but also guide the substrates to protein degradation systems when a native folding state cannot be reached (37, 38). Hsp70 is involved in the ubiquitin-proteasome system, which is the main cellular protein degradation system. Recruitment of carboxyl-terminus of Hsp70 interacting protein (CHIP), which serves as an E3 ubiquitin ligase, is a well-known function of Hsp70 in the ubiquitin-proteasome pathway (39). Hsp70 is also involved in multistep processes such as substrate unfolding, insertion into the proteasomal core and proteasome biogenesis (40, 41). Accumulation of the ubiquitinated P protein in Hsp72-knocked down cells suggests that Hsp72 plays a crucial role in degradation of the P protein after the step of ubiquitination.

The V protein was also ubiquitinated and associated with Hsp72. However, Hsp72

was not essential for the V protein degradation. The MuV P protein contains a multimerization domain at the unique C-terminal region, and forms a homo-tetramer (31), while the V protein lacks the multimerization domain and functions as a monomer (42, 43). The rate-limiting step of proteasomal degradation is the unfolding of substrates (44). Therefore, degradation of the P protein may require the support of Hsp72 due to the tetrameric structure.

In summary, the formation of IBs is a common strategy of many negative-stranded RNA viruses. The present study demonstrated for the first time the functional interaction between viral and host proteins in the IBs of MuV-infected cells. The host chaperone protein Hsp72 interacted with the MuV P protein in IBs, and targeted the MuV P protein for ubiquitin-mediated degradation. These data should provide insights into the roles of chaperone proteins in virus-infected cells.

Acknowledgments

We thank Nozomi Takeda of the Equipment Management Center (Creative Research Institution, Hokkaido University) for technical support. We also thank all the members of the Department of Virology III, NIID, for their technical advice and critical input.

This work was supported by grants from the Ministry of Education, Culture, Sports, Science and Technology (Grant-in Aid for Research Activity Start-up: 25893295) and the Ministry of Health, Labour and Welfare of Japan.

References

1. **Baskerville A, Fisher-Hoch SP, Neild GH, Dowsett AB.** 1985. Ultrastructural pathology of experimental Ebola haemorrhagic fever virus infection. J. Pathol. **147:**199-209.
2. **Carlos TS, Fearns R, Randall RE.** 2005. Interferon-induced alterations in the pattern of parainfluenza virus 5 transcription and protein synthesis and the induction of virus inclusion bodies. J. Virol. **79:**14112-14121.
3. **Lifland AW, Jung J, Alonas E, Zurla C, Crowe JE, Jr., Santangelo PJ.** 2012. Human respiratory syncytial virus nucleoprotein and inclusion bodies antagonize the innate immune response mediated by MDA5 and MAVS. J. Virol. **86:**8245-8258.
4. **Lahaye X, Vidy A, Pomier C, Obiang L, Harper F, Gaudin Y, Blondel D.** 2009.

455 Functional characterization of Negri bodies (NBs) in rabies virus-infected cells:
456 Evidence that NBs are sites of viral transcription and replication. J. Virol.
457 **83:**7948-7958.
458 5. **Heinrich BS, Cureton DK, Rahmeh AA, Whelan SP.** 2010. Protein expression
459 redirects vesicular stomatitis virus RNA synthesis to cytoplasmic inclusions.
460 PLoS Pathog. **6:**e1000958.
461 6. **Hoenen T, Shabman RS, Groseth A, Herwig A, Weber M, Schudt G, Dolnik**
462 **O, Basler CF, Becker S, Feldmann H.** 2012. Inclusion bodies are a site of
463 ebolavirus replication. J. Virol. **86:**11779-11788.
464 7. **Duc-Nguyen H, Rosenblum EN.** 1967. Immuno-electron microscopy of the
465 morphogenesis of mumps virus. J. Virol. **1:**415-429.
466 8. **Norrby E, Marusyk H, Orvell C.** 1970. Morphogenesis of respiratory syncytial
467 virus in a green monkey kidney cell line (Vero). J. Virol. **6:**237-242.
468 9. **Geisbert TW, Jahrling PB.** 1995. Differentiation of filoviruses by electron
469 microscopy. Virus Res. **39:**129-150.
470 10. **Hviid A, Rubin S, Muhlemann K.** 2008. Mumps. Lancet **371:**932-944.
471 11. **Lamb RA, Parks GD.** 2006. Paramyxoviridae: The Viruses and Their
472 Replication, p 1449-1496, *In* Knipe DM, Howley PM, Griffin DE, Lamb RA,
473 Martin MA, Roizman B, Straus SE (ed), Fields Virology, 5th ed. Lippincott
474 Williams & Wilkins, Philadelphia, PA.
475 12. **Whelan SP, Barr JN, Wertz GW.** 2004. Transcription and replication of
476 nonsegmented negative-strand RNA viruses. Curr. Top. Microbiol. Immunol.
477 **283:**61-119.
478 13. **Bukau B, Horwich AL.** 1998. The Hsp70 and Hsp60 chaperone machines. Cell
479 **92:**351-366.
480 14. **Daugaard M, Rohde M, Jaattela M.** 2007. The heat shock protein 70 family:
481 Highly homologous proteins with overlapping and distinct functions. FEBS
482 Lett. **581:**3702-3710.
483 15. **Burch AD, Weller SK.** 2004. Nuclear sequestration of cellular chaperone and
484 proteasomal machinery during herpes simplex virus type 1 infection. J. Virol.
485 **78:**7175-7185.
486 16. **Brown G, Rixon HW, Steel J, McDonald TP, Pitt AR, Graham S, Sugrue RJ.**
487 2005. Evidence for an association between heat shock protein 70 and the

488 respiratory syncytial virus polymerase complex within lipid-raft membranes
489 during virus infection. Virology **338:**69-80.
490 17. **Kaufer S, Coffey CM, Parker JS.** 2012. The cellular chaperone hsc70 is
491 specifically recruited to reovirus viral factories independently of its chaperone
492 function. J. Virol. **86:**1079-1089.
493 18. **Carsillo T, Zhang X, Vasconcelos D, Niewiesk S, Oglesbee M.** 2006. A single
494 codon in the nucleocapsid protein C terminus contributes to in vitro and in vivo
495 fitness of Edmonston measles virus. J. Virol. **80:**2904-2912.
496 19. **Lahaye X, Vidy A, Fouquet B, Blondel D.** 2012. Hsp70 protein positively
497 regulates rabies virus infection. J. Virol. **86:**4743-4751.
498 20. **Hirayama E, Atagi H, Hiraki A, Kim J.** 2004. Heat shock protein 70 is related to
499 thermal inhibition of nuclear export of the influenza virus ribonucleoprotein
500 complex. J. Virol. **78:**1263-1270.
501 21. **Li G, Zhang J, Tong X, Liu W, Ye X.** 2011. Heat shock protein 70 inhibits the
502 activity of Influenza A virus ribonucleoprotein and blocks the replication of
503 virus in vitro and in vivo. PLoS One **6:**e16546.
504 22. **Saito H, Takahashi Y, Harata S, Tanaka K, Sano T, Suto T, Yamada A,**
505 **Yamazaki S, Morita M.** 1996. Isolation and characterization of mumps virus
506 strains in a mumps outbreak with a high incidence of aseptic meningitis.
507 Microbiol. Immunol. **40:**271-275.
508 23. **Katoh H, Okamoto T, Fukuhara T, Kambara H, Morita E, Mori Y, Kamitani W,**
509 **Matsuura Y.** 2013. Japanese encephalitis virus core protein inhibits stress
510 granule formation through an interaction with Caprin-1 and facilitates viral
511 propagation. J. Virol. **87:**489-502.
512 24. **Takeuchi K, Tanabayashi K, Hishiyama M, Yamada YK, Yamada A, Sugiura**
513 **A.** 1990. Detection and characterization of mumps virus V protein. Virology
514 **178:**247-253.
515 25. **Tanabayashi K, Takeuchi K, Hishiyama M, Yamada A, Tsurudome M, Ito Y,**
516 **Sugiura A.** 1990. Nucleotide sequence of the leader and nucleocapsid protein
517 gene of mumps virus and epitope mapping with the in vitro expressed
518 nucleocapsid protein. Virology **177:**124-130.
519 26. **Tsurudome M, Yamada A, Hishiyama M, Ito Y.** 1986. Monoclonal antibodies
520 against the glycoproteins of mumps virus: fusion inhibition by anti-HN

monoclonal antibody. J. Gen. Virol. **67 (Pt 10):**2259-2265.

27. **Meng L, Mohan R, Kwok BH, Elofsson M, Sin N, Crews CM.** 1999. Epoxomicin, a potent and selective proteasome inhibitor, exhibits in vivo antiinflammatory activity. Proc. Natl. Acad. Sci. U. S. A. **96:**10403-10408.

28. **Menager P, Roux P, Megret F, Bourgeois JP, Le Sourd AM, Danckaert A, Lafage M, Prehaud C, Lafon M.** 2009. Toll-like receptor 3 (TLR3) plays a major role in the formation of rabies virus Negri Bodies. PLoS Pathog. **5:**e1000315.

29. **Mayer MP.** 2005. Recruitment of Hsp70 chaperones: a crucial part of viral survival strategies. Rev. Physiol. Biochem. Pharmacol. **153:**1-46.

30. **Munday DC, Wu W, Smith N, Fix J, Noton SL, Galloux M, Touzelet O, Armstrong SD, Dawson JM, Aljabr W, Easton AJ, Rameix-Welti MA, de Oliveira AP, Simabuco F, Ventura AM, Hughes DJ, Barr JN, Fearns R, Digard P, Eleouet JF, Hiscox JA.** 2014. Interactome analysis of the human respiratory syncytial virus RNA polymerase complex identifies protein chaperones as important co-factors that promote L protein stability and RNA synthesis. J. Virol. *In press*

31. **Cox R, Green TJ, Purushotham S, Deivanayagam C, Bedwell GJ, Prevelige PE, Luo M.** 2013. Structural and functional characterization of the mumps virus phosphoprotein. J. Virol. **87:**7558-7568.

32. **Cox R, Pickar A, Qiu S, Tsao J, Rodenburg C, Dokland T, Elson A, He B, Luo M.** 2014. Structural studies on the authentic mumps virus nucleocapsid showing uncoiling by the phosphoprotein. Proc. Natl. Acad. Sci. U. S. A. **111:**15208-15213.

33. **Bence NF, Sampat RM, Kopito RR.** 2001. Impairment of the ubiquitin-proteasome system by protein aggregation. Science **292:**1552-1555.

34. **Li X, Li H, Li XJ.** 2008. Intracellular degradation of misfolded proteins in polyglutamine neurodegenerative diseases. Brain research reviews **59:**245-252.

35. **Gray PM, Parks GD, Alexander-Miller MA.** 2001. A novel CD8-independent high-avidity cytotoxic T-lymphocyte response directed against an epitope in the phosphoprotein of the paramyxovirus simian virus 5. J. Virol. **75:**10065-10072.

36. **Gray PM, Parks GD, Alexander-Miller MA.** 2004. Modulation of CD8+ T cell avidity by increasing the turnover of viral antigen during infection. Cell. Immunol. **231:**14-19.

554 37. **Hartl FU, Hayer-Hartl M.** 2009. Converging concepts of protein folding in vitro
555 and in vivo. Nat. Struct. Mol. Biol. **16:**574-581.
556 38. **Kettern N, Dreiseidler M, Tawo R, Hohfeld J.** 2010. Chaperone-assisted
557 degradation: multiple paths to destruction. Biol. Chem. **391:**481-489.
558 39. **Ballinger CA, Connell P, Wu Y, Hu Z, Thompson LJ, Yin LY, Patterson C.**
559 1999. Identification of CHIP, a novel tetratricopeptide repeat-containing protein
560 that interacts with heat shock proteins and negatively regulates chaperone
561 functions. Mol. Cell. Biol. **19:**4535-4545.
562 40. **Esser C, Alberti S, Hohfeld J.** 2004. Cooperation of molecular chaperones with
563 the ubiquitin/proteasome system. Biochim. Biophys. Acta **1695:**171-188.
564 41. **Rosenzweig R, Glickman MH.** 2008. Chaperone-driven proteasome assembly.
565 Biochem. Soc. Trans. **36:**807-812.
566 42. **Motz C, Schuhmann KM, Kirchhofer A, Moldt M, Witte G, Conzelmann KK,**
567 **Hopfner KP.** 2013. Paramyxovirus V proteins disrupt the fold of the RNA
568 sensor MDA5 to inhibit antiviral signaling. Science **339:**690-693.
569 43. **Li T, Chen X, Garbutt KC, Zhou P, Zheng N.** 2006. Structure of DDB1 in
570 complex with a paramyxovirus V protein: viral hijack of a propeller cluster in
571 ubiquitin ligase. Cell **124:**105-117.
572 44. **Thrower JS, Hoffman L, Rechsteiner M, Pickart CM.** 2000. Recognition of the
573 polyubiquitin proteolytic signal. EMBO J. **19:**94-102.
574
575 **Figure Legends**
576 **Fig. 1.** Intracellular localizations of MuV proteins and genomic RNA. (A) Vero cells
577 infected with MuV were immunostained at 24 hr postinfection (h.p.i.) with mouse
578 anti-N (23D), anti-P (57A), anti-M (79D), anti-F (170C) or anti-HN (78) MAb and rabbit
579 anti-N, anti-V/P (T61), anti-V (T60) or anti-L (L17) PAb, followed by AF488-conjugated
580 anti-mouse IgG and AF594-conjugated anti-rabbit IgG, respectively. Cell nuclei were
581 stained with DAPI (blue). (B) Vero cells infected with MuV were immunostained at 24
582 h.p.i. with rabbit anti-V/P PAb and AF594-conjugated anti-rabbit IgG. Then, the cells
583 were subjected to fluorescence *in situ* hybridization assay to detect viral genomic RNA.
584 Cell nuclei were stained with DAPI (blue). (C and D) Vero cells transfected with
585 pCAGGS-N, P and/or L alone or in combination were immunostained at 24 hr
586 posttransfection with anti-N or anti-P MAb and anti-V/P or anti-L PAb, followed by

AF488-conjugated anti-mouse IgG and AF594-conjugated anti-rabbit IgG, respectively. Cell nuclei were stained with DAPI (blue).

Fig. 2. Identification of cellular proteins associated with the MuV P protein by FOS-tagged purification. (A) Overview of the FOS-tagged purification of cellular proteins associated with the MuV N and P protein. (B) Vero cells transfected with pCAG-N-FOS and/or pCAG-P-FOS were immunostained at 24 hr posttransfection with mouse anti-N MAb and rabbit anti-V/P PAb, followed by AF488-conjugated anti-mouse IgG and AF594-conjugated anti-rabbit IgG. Cell nuclei were stained with DAPI (blue). (C) Purified products were subjected to SDS-PAGE, followed by CBB staining. The empty vector (EV) was used as a negative control. (D) Purification of the P-FOS protein was confirmed by immunoblotting using mouse anti-FLAG MAb (M2) and rabbit anti-V/P PAb. (E) Detection of Hsp70 family proteins in the purified P-FOS complexes was performed by immunoblotting using the appropriate antibodies.

Fig. 3. Hsp72 was up-regulated and recruited to the IBs during MuV infection. (A) Summary of Hsp70 family protein candidates for binding partners of the P protein. (B) FLAG-Hsp70 proteins were coexpressed with HA-P in 293T cells, immunoprecipitated with anti-HA antibody, and immunoblotted with anti-HA and anti-FLAG antibodies. (C) Vero cells infected with MuV were immunostained at 24 hr postinfection (h.p.i.) with mouse anti-Hsp72 or anti-Hsc70 MAb and rabbit anti-MuV V/P PAb or mouse anti-P MAb and rabbit anti-GRP78 PAb, followed by the appropriated secondary Alexa-conjugated antibodies, respectively. Cell nuclei were stained with DAPI (blue). (D) Vero cells were infected with MuV at an MOI of 1.0. Cell lysates were collected at the indicated times and subjected to immunoblotting with the appropriate antibodies. (E) 293T cells were transfected with pCAGGS-P or empty vector (EV). At 24 hr postransfection, cell lysates were collected and subjected to immunoblotting with the appropriate antibodies. (F and G) Vero cells transfected with pCAGGS-P alone (F) or pCAGGS-N and -P (G) were immunostained at 24 hr posttransfection with mouse anti-Hsp72 MAb and rabbit anti-V/P PAb, followed by AF488-conjugated anti-mouse IgG and AF594-conjugated anti-rabbit IgG. Cell nuclei were stained with DAPI (blue).

Fig. 4. Determination of the regions responsible for the interaction between the P

protein and Hsp72. (A) FLAG-Hsp72 and its deletion mutants were coexpressed with HA-P in 293T cells, immunoprecipitated with anti-FLAG antibody, and immunoblotted with anti-FLAG and anti-HA antibodies. (B) HA-P and its deletion mutants were coexpressed with FLAG-Hsp72 in 293T cells, immunoprecipitated with anti-HA antibody, and immunoblotted with anti-HA and anti-FLAG antibodies. (C) FLAG-Hsp72 was coexpressed with HA-V in 293T cells, immunoprecipitated with anti-HA antibody, and immunoblotted with anti-HA and anti-FLAG antibodies.

Fig. 5. Effects of Hsp72 knockdown on MuV propagation. (A) At 48 hr posttransfection with either siHsp72 or siNC, Vero cells were inoculated with MuV at an MOI of 1.0. Cell lysates were collected at 24 hr postinfection (h.p.i.) and subjected to immunoblotting with the indicated antibodies. (B) At 48 hr posttransfection with either siHsp72 or siNC, Vero cells were inoculated with MuV at an MOI of 5.0. Total cellular RNA was extracted at 24 h.p.i. and subjected to RT using an oligo(dT) primer. The levels of N mRNA were determined by real-time PCR and calculated as percentages of the control HPRT1 mRNA level. The data are representative of three independent experiments. Error bars indicate the standard deviations of the means. (C) At 48 hr posttransfection with either siHsp72 or siNC, Vero or Huh7 cells were infected with MuV at an MOI of 0.01. The supernatants were collected at 24, 48, 72, and 96 h.p.i., and the infectious titers were determined by plaque assay in Vero cells. The results shown are from three independent experiments, with the error bars representing the standard deviations. (D) At 48 hr posttransfection with either siHsp72 or siNC, Vero cells were inoculated with MuV at an MOI of 1.0. At 24 h.p.i., the cells were fixed, permeabilized and immunostained with mouse anti-Hsp72 MAb and rabbit anti-V/P PAb, followed by AF488-conjugated anti-mouse IgG and AF594-conjugated anti-rabbit IgG. Cell nuclei were stained with DAPI (blue).

Fig. 6. Increased apoptosis in MuV-infected Hsp72 knockdown cells. (A) At 48 hr posttransfection with either siHsp72 or siNC, Vero cells were infected with MuV at an MOI of 5.0. At 24 hr postinfection (h.p.i.), the cells were fixed, permeabilized and stained with TUNEL stain. (B) TUNEL-positive cells were counted and expressed as percentages of total cells (n > 1,000). Total cells were calculated by DAPI staining. (C) At 48 hr posttransfection with either siHsp72 or siNC, Vero cells were inoculated with

MuV at an MOI of 5.0. At 24 h.p.i., caspase 3/7 activity was measured, and relative caspase 3/7 activity was calculated by normalization with cell viability.

Fig. 7. Ubiquitination of MuV P and V proteins. (A) 293T cells were transfected with a plasmid encoding HA-Ub and infected with MuV. At 24 h.p.i., the cells were treated with 10 μM of MG-132 for 5 hr, and then the cell lysates were subjected to immunoprecipitation assay with anti-V/P antibody, followed by immunoblotting with the appropriate antibodies. (B) At 24 h.p.i., Vero cells infected with MuV were treated with 10 μM of MG-132 for 5 hr, and then the cell lysates were subjected to immunoprecipitation assay with anti-V/P antibody, followed by immunoblotting with the appropriate antibodies.

Fig. 8. Hsp72 regulates the P protein degradation through the ubiquitin-proteasome system. (A) At 48 hr posttransfection with either siHsp72 or siNC, 293T cells were transfected with a plasmid encoding HA-Ub and infected with MuV. At 24 hr postinfection (h.p.i.), the cells were treated with 10 μM of MG-132 for 5 hr, and then the cell lysates were subjected to immunoprecipitation assay with anti-V/P antibody, followed by immunoblotting with anti-HA and anti-V/P antibodies. (B) At 48 hr posttransfection with either siHsp72 or siNC, 293T cells were transfected with plasmids pCAGPM-HA-Ub and pCAGGS-P or -V, respectively. After 24 hr, the cell lysates were subjected to immunoprecipitation assay with anti-V/P antibody, followed by immunoblotting with anti-HA and anti-V/P antibodies. (C) At 48 hr posttransfection with either siHsp72 or siNC, Vero cells were infected with MuV. At 24 h.p.i., the cells were treated with MG-132 (10 μM), Lactacystin (5 μM), Epoxomicin (10 μM) or DMSO for 2 hr. Then, 50 μg/ml of CHX was added, and the cell lysates were collected at the indicated times. The expression levels of the P and V proteins were detected by immunoblotting with anti-V/P antibody.

Katoh et al., Fig. 1

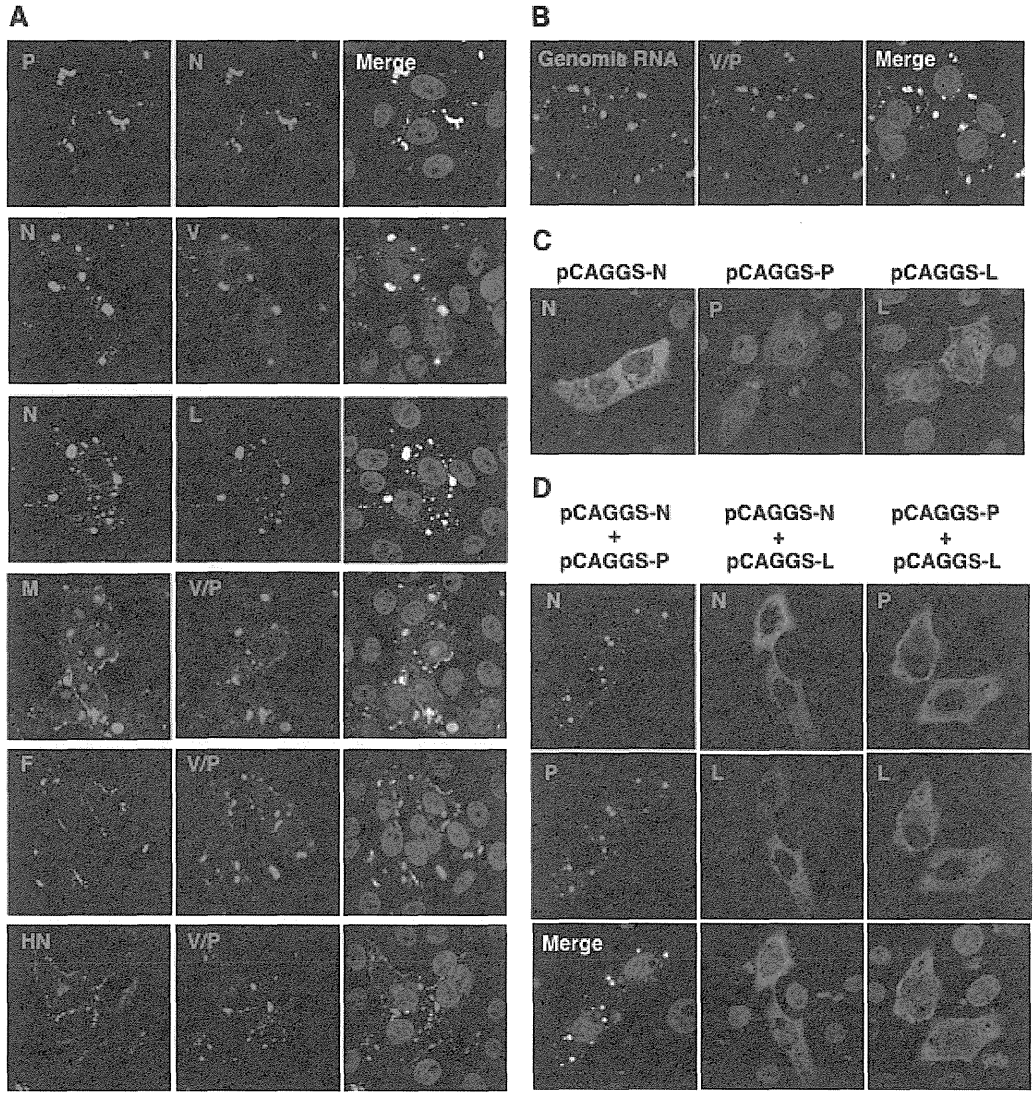

Fig. 1. Intracellular localizations of MuV proteins and genomic RNA. (A) Vero cells infected with MuV were immunostained at 24 hr postinfection (h.p.i.) with mouse anti-N (23D), anti-P (57A), anti-M (79D), anti-F (170C) or anti-HN (78) MAb and rabbit anti-N, anti-V/P (T61), anti-V (T60) or anti-L (L17) PAb, followed by AF488-conjugated anti-mouse IgG and AF594-conjugated anti-rabbit IgG, respectively. Cell nuclei were stained with DAPI (blue). (B) Vero cells infected with MuV were immunostained at 24 h.p.i. with rabbit anti-V/P PAb and AF594-conjugated anti-rabbit IgG. Then, the cells were subjected to fluorescence *in situ* hybridization assay to detect viral genomic RNA. Cell nuclei were stained with DAPI (blue). (C and D) Vero cells transfected with pCAGGS-N, P and/or L alone or in combination were immunostained at 24 hr posttransfection with anti-N or anti-P MAb and anti-V/P or anti-L PAb, followed by AF488-conjugated anti-mouse IgG and AF594-conjugated anti-rabbit IgG, respectively. Cell nuclei were stained with DAPI (blue).

Katoh et al., Fig. 2

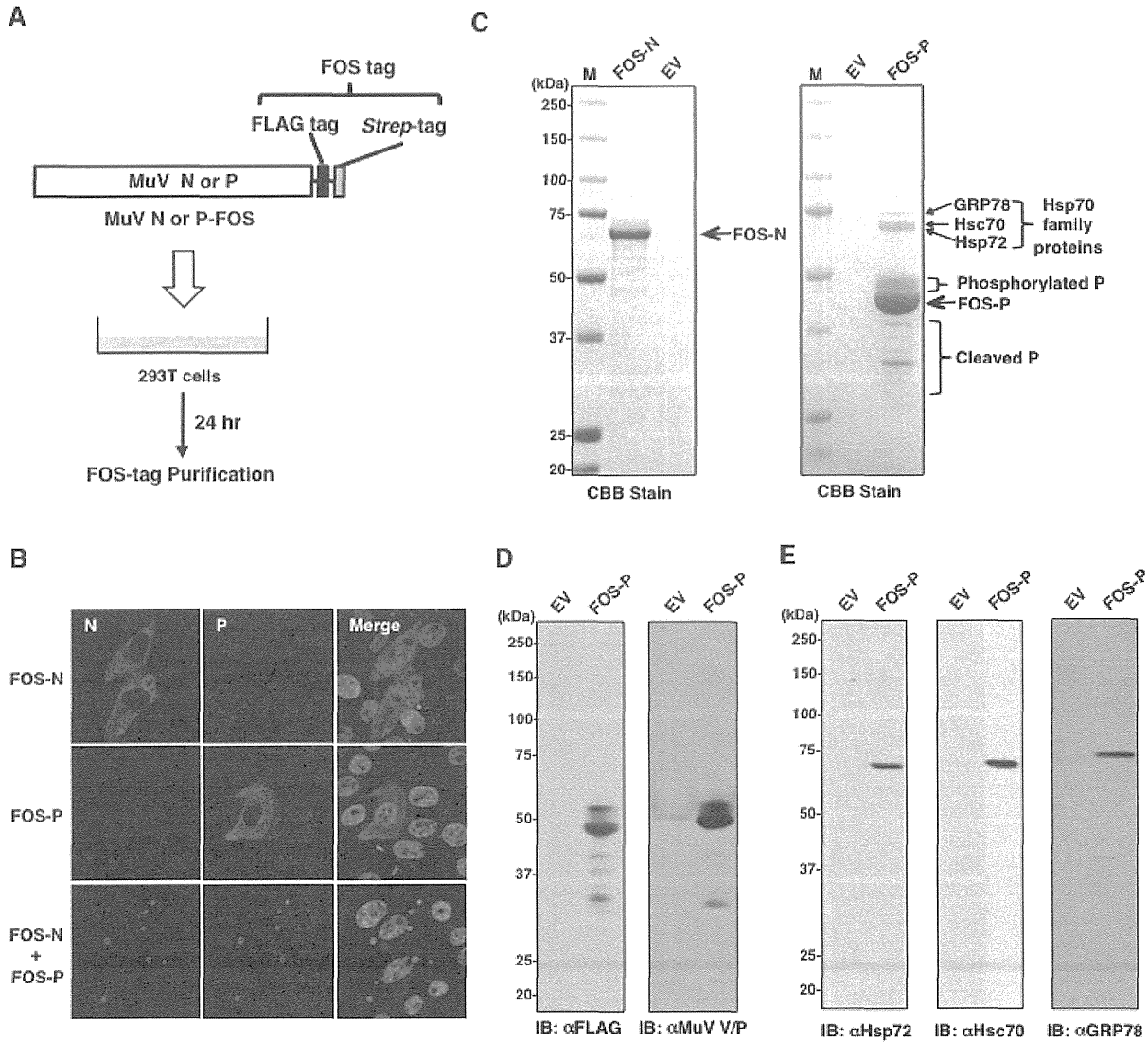

Fig. 2. *Identification of cellular proteins associated with the MuV P protein by FOS-tagged purification.* (A) Overview of the FOS-tagged purification of cellular proteins associated with the MuV N and P protein. (B) Vero cells transfected with pCAG-N-FOS and/or pCAG–P-FOS were immunostained at 24 hr posttransfection with mouse anti-N MAb and rabbit anti-V/P PAb, followed by AF488-conjugated anti-mouse IgG and AF594-conjugated anti-rabbit IgG. Cell nuclei were stained with DAPI (blue). (C) Purified products were subjected to SDS-PAGE, followed by CBB staining. The empty vector (EV) was used as a negative control. (D) Purification of the P-FOS protein was confirmed by immunoblotting using mouse anti-FLAG MAb (M2) and rabbit anti-V/P PAb. (E) Detection of Hsp70 family proteins in the purified P-FOS complexes was performed by immunoblotting using the appropriate antibodies.

Katoh et al., Fig. 3

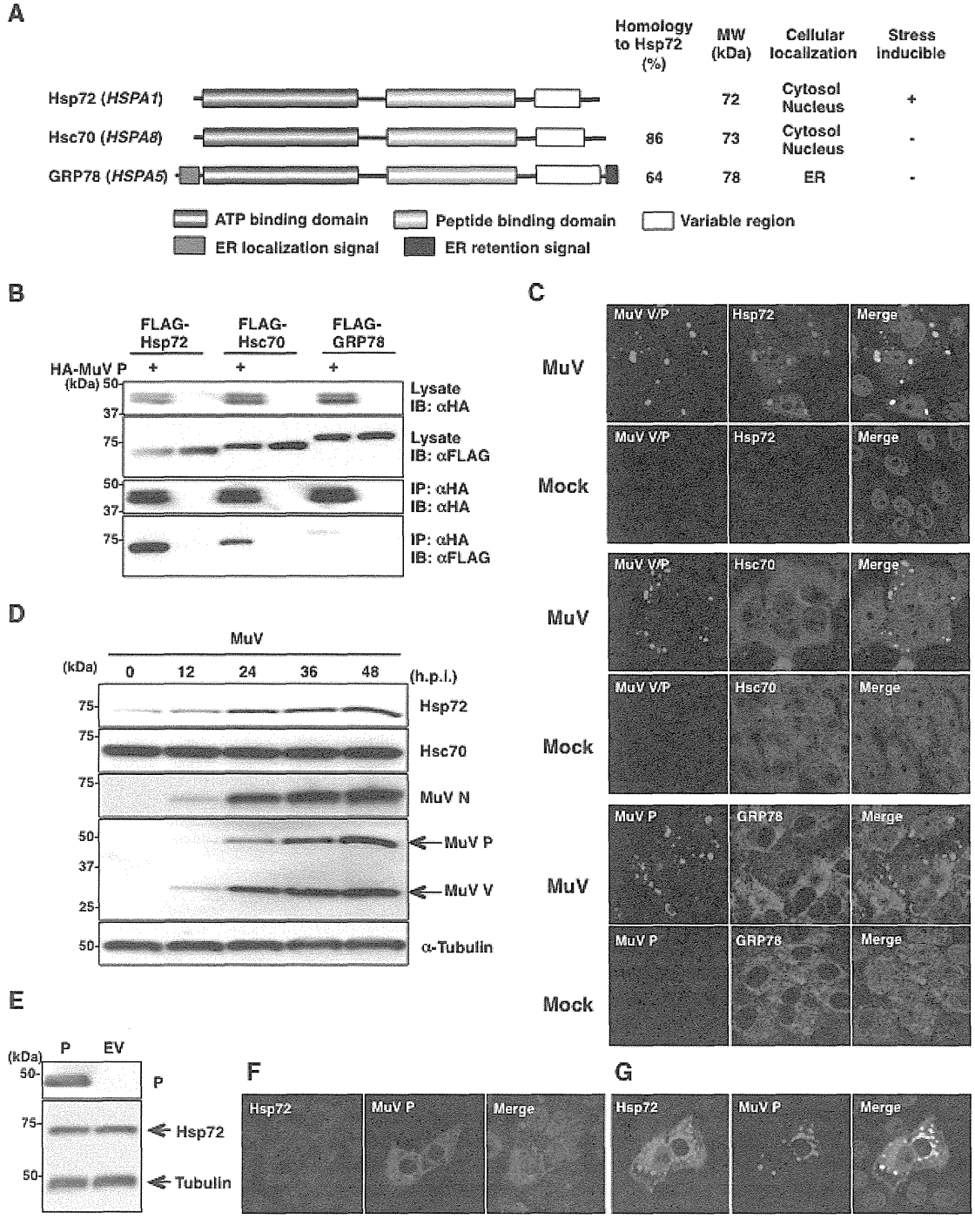

Fig. 3. Hsp72 was up-regulated and recruited to the IBs during MuV infection. (A) Summary of Hsp70 family protein candidates for binding partners of the P protein. (B) FLAG-Hsp70 proteins were coexpressed with HA-P in 293T cells, immunoprecipitated with anti-HA antibody, and immunoblotted with anti-HA and anti-FLAG antibodies. (C) Vero cells infected with MuV were immunostained at 24 hr postinfection (h.p.i.) with mouse anti-Hsp72 or anti-Hsc70 MAb and rabbit anti-MuV V/P PAb or mouse anti-P MAb and rabbit anti-GRP78 PAb, followed by the appropriated secondary Alexa-conjugated antibodies, respectively. Cell nuclei were stained with DAPI (blue). (D) Vero cells were infected with MuV at an MOI of 1.0. Cell lysates were collected at the indicated times and subjected to immunoblotting with the appropriate antibodies. (E) 293T cells were transfected with pCAGGS-P or empty vector (EV). At 24 hr postransfection, cell lysates were collected and subjected to immunoblotting with the appropriate antibodies. (F and G) Vero cells transfected with pCAGGS-P alone (F) or pCAGGS-N and -P (G) were immunostained at 24 hr posttransfection with mouse anti-Hsp72 MAb and rabbit anti-V/P PAb, followed by AF488-conjugated anti-mouse IgG and AF594-conjugated anti-rabbit IgG. Cell nuclei were stained with DAPI (blue).

Katoh et al., Fig. 4

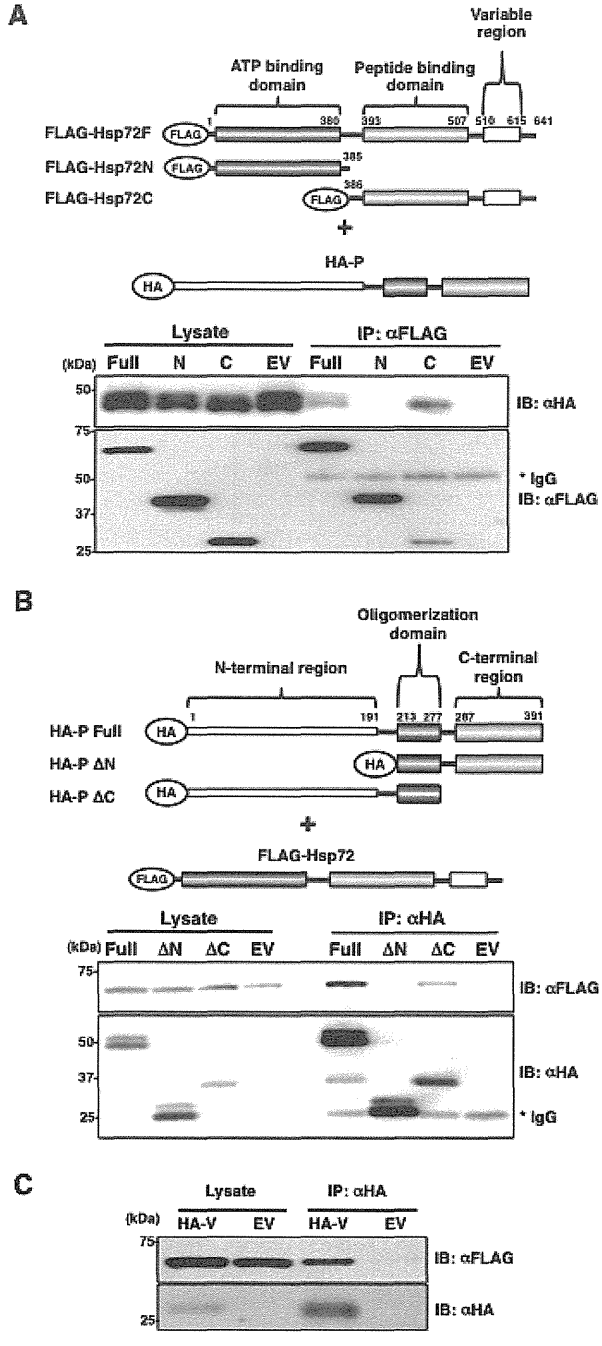

Fig. 4. Determination of the regions responsible for the interaction between the P protein and Hsp72. (A) FLAG-Hsp72 and its deletion mutants were coexpressed with HA-P in 293T cells, immunoprecipitated with anti-FLAG antibody, and immunoblotted with anti-FLAG and anti-HA antibodies. (B) HA-P and its deletion mutants were coexpressed with FLAG-Hsp72 in 293T cells, immunoprecipitated with anti-HA antibody, and immunoblotted with anti-HA and anti-FLAG antibodies. (C) FLAG-Hsp72 was coexpressed with HA-V in 293T cells, immunoprecipitated with anti-HA antibody, and immunoblotted with anti-HA and anti-FLAG antibodies.

Katoh et al., Fig. 5

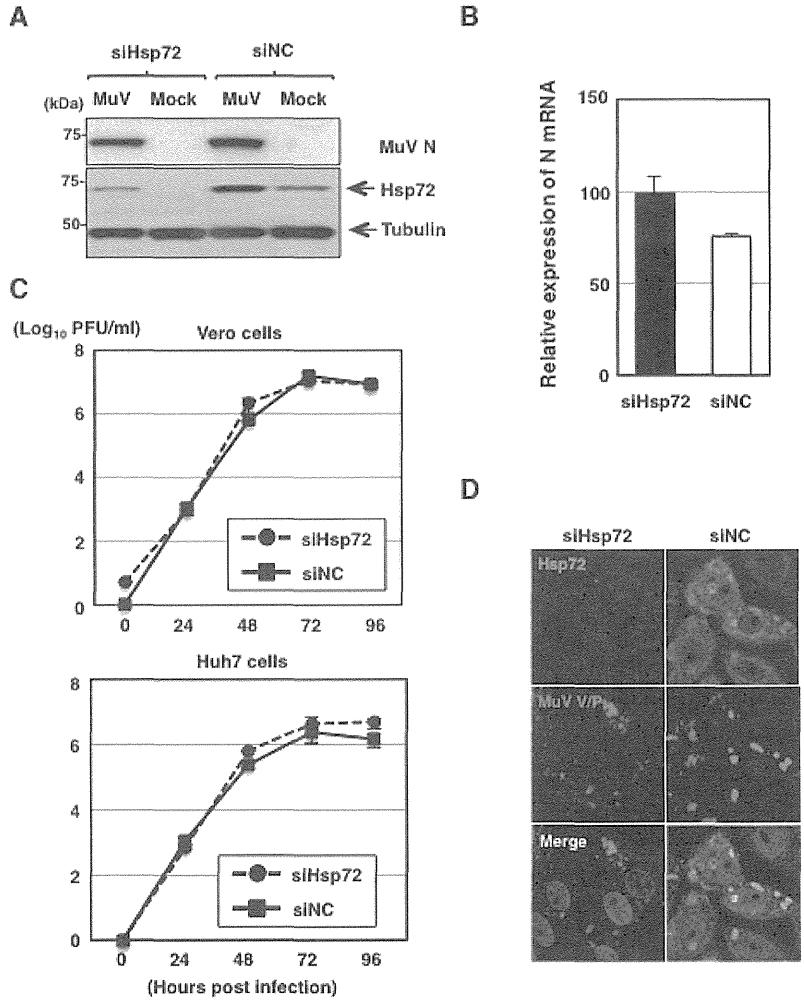

Fig. 5. Effects of Hsp72 knockdown on MuV propagation. (A) At 48 hr posttransfection with either siHsp72 or siNC, Vero cells were inoculated with MuV at an MOI of 1.0. Cell lysates were collected at 24 hr postinfection (h.p.i.) and subjected to immunoblotting with the indicated antibodies. (B) At 48 hr posttransfection with either siHsp72 or siNC, Vero cells were inoculated with MuV at an MOI of 5.0. Total cellular RNA was extracted at 24 h.p.i. and subjected to RT using an oligo(dT) primer. The levels of N mRNA were determined by real-time PCR and calculated as percentages of the control HPRT1 mRNA level. The data are representative of three independent experiments. Error bars indicate the standard deviations of the means. (C) At 48 hr posttransfection with either siHsp72 or siNC, Vero or Huh7 cells were infected with MuV at an MOI of 0.01. The supernatants were collected at 24, 48, 72, and 96 h.p.i., and the infectious titers were determined by plaque assay in Vero cells. The results shown are from three independent experiments, with the error bars representing the standard deviations. (D) At 48 hr posttransfection with either siHsp72 or siNC, Vero cells were inoculated with MuV at an MOI of 1.0. At 24 h.p.i., the cells were fixed, permeabilized and immunostained with mouse anti-Hsp72 MAb and rabbit anti-V/P PAb, followed by AF488-conjugated anti-mouse IgG and AF594-conjugated anti-rabbit IgG. Cell nuclei were stained with DAPI (blue).

Katoh et al., Fig. 6

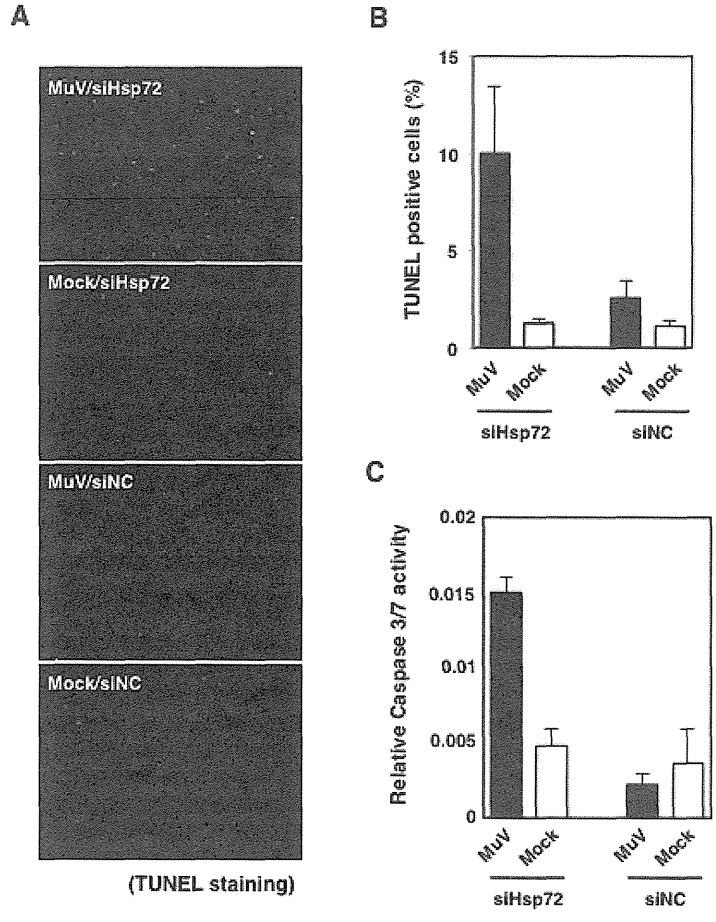

Fig. 6. Increased apoptosis in MuV-infected Hsp72 knockdown cells. (A) At 48 hr posttransfection with either siHsp72 or siNC, Vero cells were infected with MuV at an MOI of 5.0. At 24 hr postinfection (h.p.i.), the cells were fixed, permeabilized and stained with TUNEL stain. (B) TUNEL-positive cells were counted and expressed as percentages of total cells ($n > 1,000$). Total cells were calculated by DAPI staining. (C) At 48 hr posttransfection with either siHsp72 or siNC, Vero cells were inoculated with MuV at an MOI of 5.0. At 24 h.p.i., caspase 3/7 activity was measured, and relative caspase 3/7 activity was calculated by normalization with cell viability.

Katoh et al., Fig. 7

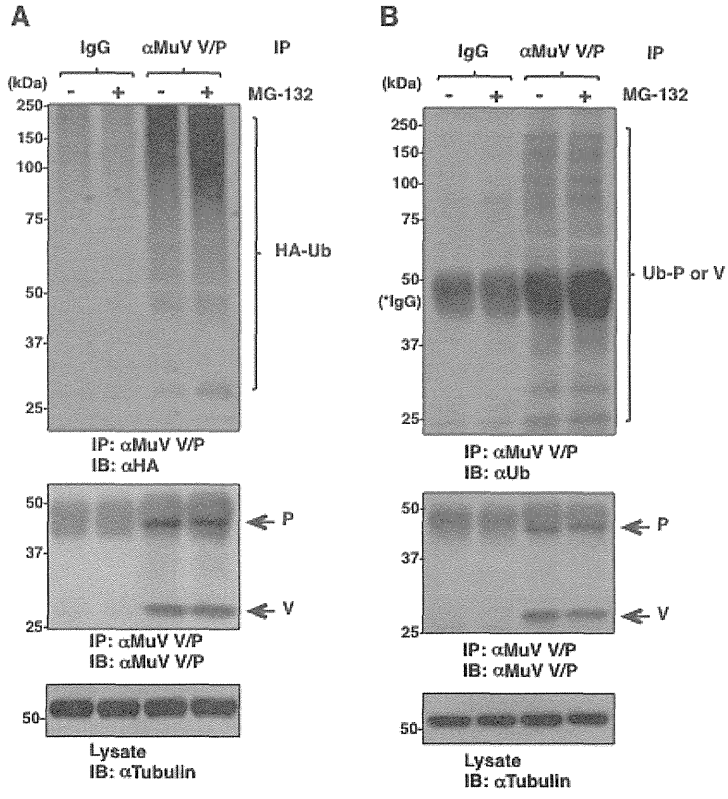

Fig. 7. Ubiquitination of MuV P and V proteins. (A) 293T cells were transfected with a plasmid encoding HA-Ub and infected with MuV. At 24 h.p.i., the cells were treated with 10 μM of MG-132 for 5 hr, and then the cell lysates were subjected to immunoprecipitation assay with anti-V/P antibody, followed by immunoblotting with the appropriate antibodies. (B) At 24 h.p.i., Vero cells infected with MuV were treated with 10 μM of MG-132 for 5 hr, and then the cell lysates were subjected to immunoprecipitation assay with anti-V/P antibody, followed by immunoblotting with the appropriate antibodies.

Katoh et al., Fig. 8

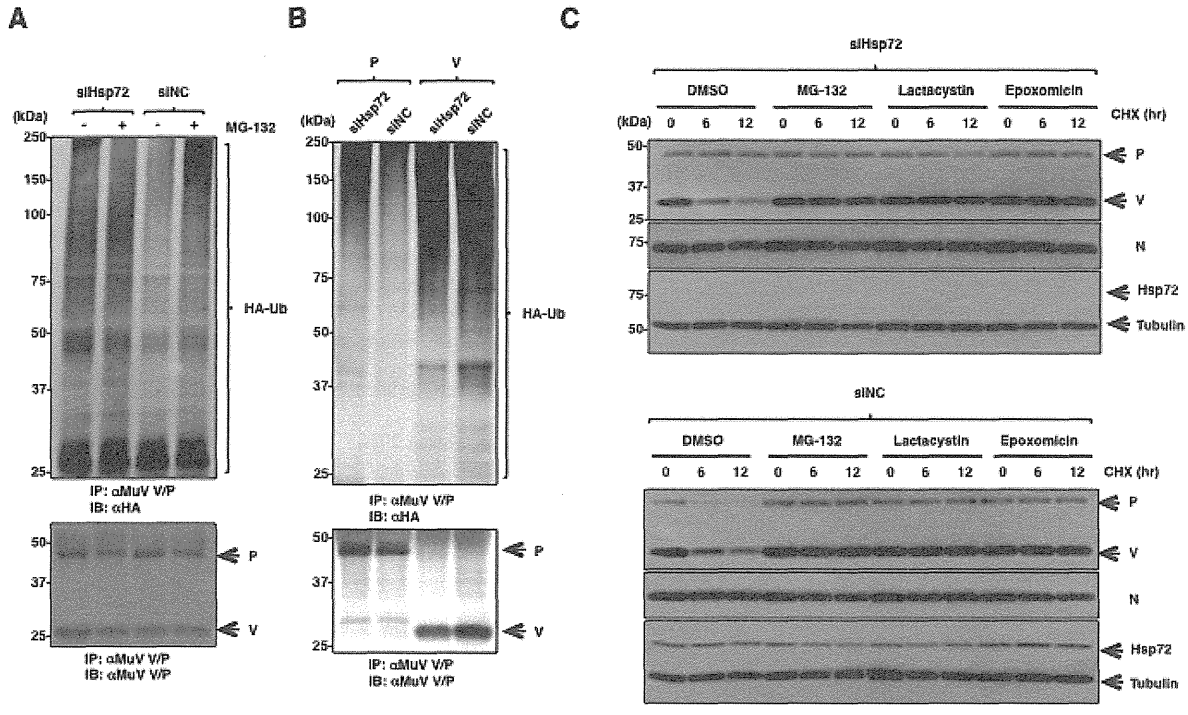

Fig. 8. Hsp72 regulates the P protein degradation through the ubiquitin-proteasome system. (A) At 48 hr posttransfection with either siHsp72 or siNC, 293T cells were transfected with a plasmid encoding HA-Ub and infected with MuV. At 24 hr postinfection (h.p.i.), the cells were treated with 10 μM of MG-132 for 5 hr, and then the cell lysates were subjected to immunoprecipitation assay with anti-V/P antibody, followed by immunoblotting with anti-HA and anti-V/P antibodies. (B) At 48 hr posttransfection with either siHsp72 or siNC, 293T cells were transfected with plasmids pCAGPM-HA-Ub and pCAGGS-P or -V, respectively. After 24 hr, the cell lysates were subjected to immunoprecipitation assay with anti-V/P antibody, followed by immunoblotting with anti-HA and anti-V/P antibodies. (C) At 48 hr posttransfection with either siHsp72 or siNC, Vero cells were infected with MuV. At 24 h.p.i., the cells were treated with MG-132 (10 μM), Lactacystin (5 μM), Epoxomicin (10 μM) or DMSO for 2 hr. Then, 50 μg/ml of CHX was added, and the cell lysates were collected at the indicated times. The expression levels of the P and V proteins were detected by immunoblotting with anti-V/P antibody.

Hindawi Publishing Corporation
BioMed Research International
Volume 2014, Article ID 902478, 13 pages
http://dx.doi.org/10.1155/2014/902478

Research Article

Combined Cytolytic Effects of a Vaccinia Virus Encoding a Single Chain Trimer of MHC-I with a Tax-Epitope and Tax-Specific CTLs on HTLV-I-Infected Cells in a Rat Model

Takashi Ohashi,[1] Takafumi Nakamura,[2] Minoru Kidokoro,[3] Xianfeng Zhang,[1] and Hisatoshi Shida[1]

[1] *Division of Molecular Virology, Institute for Genetic Medicine, Hokkaido University, Kita 15, Nishi 7, Kita-ku, Sapporo, Hokkaido 060-0815, Japan*
[2] *Division of Integrative Bioscience, Department of Biomedical Science, Institute of Regenerative Medicine and Biofunction, Graduate School of Medical Science, Tottori University, Yonago, Tottori 683-8503, Japan*
[3] *Department of Virology III, National Institute of Infectious Diseases, Musashimurayama, Tokyo 208-0011, Japan*

Correspondence should be addressed to Takashi Ohashi; ohashi-t@igm.hokudai.ac.jp

Received 12 December 2013; Accepted 20 February 2014; Published 27 March 2014

Academic Editor: Masahisa Jinushi

Adult T cell leukemia (ATL) is a malignant lymphoproliferative disease caused by human T cell leukemia virus type I (HTLV-I). To develop an effective therapy against the disease, we have examined the oncolytic ability of an attenuated vaccinia virus (VV), LC16m8Δ (m8Δ), and an HTLV-I Tax-specific cytotoxic T lymphocyte (CTL) line, 4O1/C8, against an HTLV-I-infected rat T cell line, FPM1. Our results demonstrated that m8Δ was able to replicate in and lyse tumorigenic FPM1 cells but was incompetent to injure 4O1/C8 cells, suggesting the preferential cytolytic activity toward tumor cells. To further enhance the cytolysis of HTLV-I-infected cells, we modified m8Δ and obtained m8Δ/RT1AlSCTax180L, which can express a single chain trimer (SCT) of rat major histocompatibility complex class I with a Tax-epitope. Combined treatment with m8Δ/RT1AlSCTax180L and 4O1/C8 increased the cytolysis of FPM1V.EFGFP/8R cells, a CTL-resistant subclone of FPM1, compared with that using 4O1/C8 and m8Δ presenting an unrelated peptide, suggesting that the activation of 4O1/C8 by m8Δ/RT1AlSCTax180L further enhanced the killing of the tumorigenic HTLV-I-infected cells. Our results indicate that combined therapy of oncolytic VVs with SCTs and HTLV-I-specific CTLs may be effective for eradication of HTLV-I-infected cells, which evade from CTL lysis and potentially develop ATL.

1. Introduction

Human T cell leukemia virus type I (HTLV-I) is etiologically linked to adult T cell leukemia (ATL) [1, 2] and a chronic progressive neurological disorder termed HTLV-I-associated myelopathy/tropical spastic paraparesis (HAM/TSP) [3, 4]. HTLV-I genome contains a unique 3′ region, designated as pX, which encodes the viral transactivator protein, Tax [5]. It is speculated that Tax plays a central role in HTLV-I associated immortalization and transformation of T cells, which may lead to the development of ATL [6]. In addition, Tax is also known as a major target protein recognized by cytotoxic T lymphocyte (CTL) of HTLV-I carriers [7]. A number of studies have reported that CTL responses were activated in HAM/TSP patients but were weak in ATL patients, suggesting that the T cell response could be one of the important determinants of the disease manifestation [8]. Since HTLV-I Tax-specific CTL can recognize and lyse ATL cells in vitro [9], it is conceivable that the low CTL activity in ATL patients is disadvantageous as it may allow uncontrolled proliferation and evolution of HTLV-I-infected cells in vivo. Indeed, Hasegawa et al. have reported that oral HTLV-I-infection induced HTLV-I-specific T cell tolerance and caused an elevation of the proviral loads and that reimmunization resulted in the recovery of the virus-specific T cell responses and the decrease of the proviral loads in a rat model system [10]. In addition, the development of ATL has been reported in HTLV-I carriers who received immunosuppressants during organ transplantation [11]. Increase of Tax-specific CTLs observed in ATL patients treated successfully

with allogeneic hematopoietic stem cell transplantation (allo-HSCT) also suggests the importance of virus-specific CTLs to control the disease [12]. Thus, immune therapies to activate HTLV-I-specific CTLs are considered as novel attempts for the treatment of ATL. In this regard, we have previously demonstrated the therapeutic effect of Tax-coding DNA or peptide in a rat model of ATL-like disease [13, 14]. In addition, it has been recently reported that autologous Tax-specific CTLs showed therapeutic benefits in an animal model using NOG mice bearing primary ATL cells, suggesting the possible translation into a clinical use [15].

To improve therapeutic effects of immune therapy, it is important to consider tumor microenvironment, because tumor cells often induce a microenvironment, which favors the development of immunosuppressive populations of immune cells, such as myeloid-derived suppressor cells and regulatory T cells [16]. In HTLV-I carriers and ATL patients, various kinds of immunosuppressive events have been reported, indicating the importance of developing new strategies to eliminate HTLV-I-infected cells in such immunosuppressive environments [8]. One of powerful strategies to lyse tumor cells in an immunosuppressive microenvironment would be the use of replication-competent oncolytic viruses, because oncolytic virotherapy has been known to induce both direct tumor killing and local proinflammatory environments that help to reverse the immunosuppressive environment of tumors [17, 18]. As for HTLV-I infection, vesicular stomatitis virus (VSV) has been reported to have oncolytic activity against primary ATL cells [19]. Vaccinia virus (VV) has been also shown to be a good candidate for oncolytic virotherapies [20]. It has been already assessed in clinical trials and shown to selectively infect, replicate, and express transgene products in cancer tissues without damaging normal tissues [21]. We have previously constructed a highly attenuated VV, LC16m8Δ (m8Δ), which is genetically more stable than LC16m8 (m8), a naturally occurring counterpart of m8Δ, and less pathogenic than its parental LC16mO (mO) due to the deletion of B5R gene [22]. The safety of m8Δ has been already confirmed in clinical use of its natural counterpart; m8 has been safely administered to approximately 100,000 infants and 3,000 adults for smallpox vaccination and induced levels of immunity similar to those of the original Lister strain without serious side effects [23]. Moreover, Hikichi et al. have recently reported the oncolytic potential of m8Δ with regulated expression of B5R [24]. Thus, the application of m8Δ for the elimination of HTLV-I-infected cells should be possible.

It is well known that HTLV-I viral protein expression is suppressed in infected cells in the peripheral blood of the virus-infected individuals, probably due to either unidentified suppression mechanisms of HTLV-I expression or genetic and epigenetic changes in the viral genome [8]. This reduction of viral protein expression may cause the decrease of anti-HTLV-I immune responses. Downregulation of major histocompatibility complex class I (MHC-I) could also lead to the evasion of HTLV-I-infected cells from the virus-specific CTLs [25]. Thus, strategies to overcome the repression of viral antigen presentation in HTLV-I infected individuals should be also required to establish effective anti-HTLV-I therapies. Improving the ability to present antigen to proper CTLs could be one possible way to overcome the problem. Single chain trimers (SCTs) of MHC-I have been reported to possess the strong potential to stimulate antigen-specific T cells [26, 27]. In this system, all three components of MHC-I complexes, such as an antigen peptide, β_2-microglobulin (β_2m), and MHC-I heavy chain, were covalently attached with flexible linkers. By connecting together the three components into a single chain chimeric protein, a complicated cellular machinery of antigen processing can be bypassed, leading to stable cell surface expression of MHC-I coupled with an antigenic peptide of interest. It has been recently reported that SCT-expressing DNA vaccine is able to break immune tolerance against self-antigen from melanoma, further supporting the potential of SCTs to clinical applications [28]. By applying SCT system to a rat model of HTLV-I infection, we have previously developed an activation and detection system of Tax-specific rat T cells and showed that SCTs with a Tax-epitope specifically recognize and activate Tax-specific CTLs [29]. In this study, to further improve the efficacy of CTL activation by SCTs, m8Δ was selected as a vector to express SCTs on the surface of HTLV-I-infected cells. Introduction of SCT coding sequence into the genome of m8Δ could generate novel therapeutic VVs, which possess abilities to both lyse tumor cells and activate tumor-specific CTLs. We further examined the combination effects of Tax-specific CTLs and m8Δ expressing SCT against CTL-resistant HTLV-I-infected cells. Our results suggested the possible application of the combined use of oncolytic viruses presenting tumor antigens and tumor-specific CTLs for the treatments against tumors including ATL.

2. Materials and Methods

2.1. Cells and Viruses. An HTLV-I-immortalized cell line, FPM1, was previously established by cocultivating thymocytes of an F344/N Jcl-rnu/+ rat (Clea Japan, Inc. Tokyo, Japan) with HTLV-I producing human cell line, MT-2, which was treated with mitomycin C (50 μg/mL) for 30 min at 37°C [30]. FPM1V.EFGFP, FPM1V.EFGFP/8R, and 4O1/C8 cells were established as previously described [25]. FPM1V.EFGFP was a subclone of FPM1 cells, which stably expresses EGFP. FPM1V.EFGFP/8R cells were generated from FPM1V.EFGFP cells, by continuously cultivating with a Tax-specific CTL, 4O1/C8, and obtained an ability to evade from CTL killing by 4O1/C8 cells. FPM1 and its subclones were maintained in RPMI 1640 with 10% heat-inactivated FCS (Sigma-Aldrich, St. Louis, MO), 55 μM of 2-mercaptoethanol (Gibco, Grand Island, NY), penicillin, and streptomycin. The 4O1/C8 cells were established from an F344/N Jcl-rnu/+ rat inoculated with Tax-coding DNA and were maintained in RPMI 1640 medium with 10% FCS, 55 μM of 2-mercaptoethanol, and 20 U of IL-2 (PEPROTECH, London, UK) per mL with periodical stimulation using formalin-fixed FPM1 cells every 4 weeks. A rabbit kidney epithelial cell line, RK13, was cultured in RPMI1640 supplemented with 10% FCS. Hamster BHK cells were cultured in D-MEM supplemented with 10% FCS. Canarypox virus (a kind gift of National Institute of Animal Health) [31], mO, m8Δ [22], and LC16 m8ΔVNC110 that harbors multiple cloning site in the HA gene of m8Δ